Fiber-optic magnetometry with randomly oriented spins

I. V. Fedotov,[1,2,3] L. V. Doronina-Amitonova,[1,3] D. A. Sidorov-Biryukov,[1,3] N. A. Safronov,[1,3] A. O. Levchenko,[4] S. A. Zibrov,[4] S. Blakley,[2] H. Perez,[2] A. V. Akimov,[3] A. B. Fedotov,[1,3] P. Hemmer,[2] K. Sakoda,[5] V. L. Velichansky,[4] M. O. Scully,[2,6] and A. M. Zheltikov[1,2,3,*]

[1]*Physics Department, International Laser Center, M.V. Lomonosov Moscow State University, Moscow 119992, Russia*

[2]*Texas A&M University, College Station, Texas 77843, USA*

[3]*Russian Quantum Center, Skolkovo 1430125, Moscow Region, Russia*

[4]*P.N. Lebedev Physical Institute, Russian Academy of Sciences, Moscow 119991, Russia*

[5]*National Institute for Materials Science, Tsukuba 305-0044, Japan*

[6]*Princeton University, Princeton, New Jersey 08544-5263, USA*

**Corresponding author: zheltikov@physics.msu.ru*

Received August 19, 2014; revised October 15, 2014; accepted October 15, 2014; posted October 16, 2014 (Doc. ID 221280); published December 1, 2014

We demonstrate fiber-optic magnetometry using a random ensemble of nitrogen-vacancy (NV) centers in nanodiamond coupled to a tapered optical fiber, which provides a waveguide delivery of optical fields for the initialization, polarization, and readout of the electron spin in NV centers. © 2014 Optical Society of America

OCIS codes: (060.2370) Fiber optics sensors; (230.0230) Optical devices.
http://dx.doi.org/10.1364/OL.39.006755

A nitrogen-vacancy (NV) color center in diamond is a unique solid-state quantum system [1–3], where the electron spin can be manipulated, polarized, and read out at room temperature using electromagnetic fields. Due to their remarkable electron-spin properties, NV centers offer much promise as solid-state qubits [2–5], single-photon sources [6], efficient contrast agents for superresolution optical microscopy [7,8], quantum sensors for nanoscale thermometry of living cells [9], and photostable, nonbleaching markers for bioimaging [10]. The sensitivity of the electron spin in an NV center to an external magnetic field has been recently shown to enable a new approach in magnetometry, allowing weak magnetic fields to be detected and imaged with an unprecedented spatial resolution and a remarkable sensitivity [11–14].

Integration of NV-based quantum sensors with optical fibers would be tremendously beneficial for a broad class of applications of NV-center-based magnetometry, including quantum technologies, neurosciences, and biomedical diagnostics. As a part of the earlier work in this direction, a variety of technologies enabling the embedding of diamond nanoparticles with NV centers into specially designed optical fibers have been developed [15–17] and ultracompact fiber-optic probes integrating NV quantum sensors with a waveguide delivery of optical and microwave fields have been demonstrated [18].

In the well-established protocol of NV-center-based optical magnetometry, NV spins with well-defined orientation, found in single NV centers [13,14] or NV centers in a crystal lattice [12], serve as ultrahigh-precision magnetometers. In this work, a different approach to NV-center-based optical magnetometry is demonstrated and implemented in the fiber format. We will show below in this Letter that ensembles of randomly oriented NV spins can enable, when manipulated by a microwave field, a compact and practical, albeit less sensitive scheme of optical magnetometry, which is ideally suited for fiber-format metrology and tip-assisted ultrahigh-resolution microscopy. While in the earlier demonstration of NV-based magnetometry with nanodiamond-covered tapered fibers [17], a single-NV-center spin was initialized by a free-space laser beam, our experiments show that, with a careful discrimination of the spin readout return against the background emission from the fiber, nanodiamond-covered tapered-fiber probes can support a full waveguide coupling of excitation and readout radiation to the spins of multiple NV centers, providing a waveguide delivery of optical fields for spin initialization, polarization, and readout. Moreover, the optical readout return from multiple NV centers has a much higher intensity, compared to a single NV center, simplifying the detection of this signal. Finally, experiments presented below in this Letter show that tapered-fiber probes coupled to multiple NV centers with randomly oriented spins provide a noticeably higher sensitivity of magnetic-field measurements relative to a tapered-fiber probe with a single NV center.

In our experiments, tapered fibers were produced by heating and drawing conventional telecommunication optical fibers on a standard fusion fiber splicer to fiber taper waist diameters ranging from 0.5 to 5 μm and conical transition lengths from 0.05 to 10 mm. Nanodiamond with NV centers was deposited on the fiber taper [Figs. 1(a) and 1(b)] as the fiber was dipped into a water suspension of diamond nanoparticles with an average diameter of 300 nm and a relative size variance of about

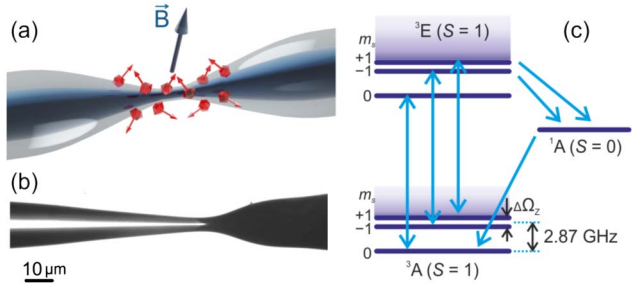

Fig. 1. Sketch (a) and a microscope image (b) of a fiber taper covered with diamond nanoparticles with NV centers. (c) Diagram of energy levels of an NV center involved in magnetic-field sensing.

30% and dried out at an elevated temperature during four hours.

For optical initialization of NV centers in nanodiamond, the 50-mW, 532-nm second-harmonic output of a continuous-wave Nd: YAG laser is coupled to the tapered-fiber probe through a standard fiber-optic coupler and is delivered to the nanodiamond-coated fiber taper, propagating first through the intact optical fiber region and then down the conical transition of the taper [Figs. 1(b) and 2]. This laser field couples to NV centers in nanodiamond through the evanescent field of fiber-taper modes [Fig. 2], promoting electrons from the ^3A ground state to the ^3E excited state [Fig. 1(c)] and giving rise to photoluminescence (PL) of NV centers. The PL emitted by laser-initialized NV centers within the 630–800-nm wavelength range [Fig. 1(c)] is evanescent-field-coupled to the fiber taper and is delivered to a photodetection system in the opposite direction, first along the fiber taper and then through the intact stretch of the optical fiber (Fig. 2). The PL readout is coupled out of the tapered-fiber probe through a standard fiber coupler. The detection system used in our experiments consists of a silicon photodiode, a low-noise preamplifier, and a lock-in amplifier. Since standard fiber couplers are used to couple optical radiation in and out of the tapered-fiber probe, no extra requirements to the accuracy of optical adjustment or the acceptable level of mechanical vibrations are imposed, except those typical of a standard fiber-optic experiment.

In Fig. 3(b), we present the spectrum of the PL response from NV centers in nanodiamond deposited on the fiber taper measured in a separate experiment, where a freely propagating 532-nm laser beam was focused on the nanodiamond-covered fiber taper and the PL signal was collected by a free-space lens [Fig. 3(a)]. This PL spectrum exhibits a characteristic zero-phonon line at approximately 637 nm, observed against a broad phonon-sideband line, stretching down to 800 nm. When the fiber probe is used to deliver the 532-nm laser beam [Fig. 2], the PL signal from NV centers is partially masked by intense background emission from the optical fiber induced by 532-nm radiation, which considerably modifies the spectra recorded in experiments [Fig. 4(a)]. Experiments with an external magnetic field B help discriminate the B-dependent part of the recorded spectra (cf. red and green lines in [Fig. 4(a)]) and quantify the level of background, which is estimated at approximately 30% of the total recorded signal within the 630750-nm wavelength range. For accurate magnetic field measurements,

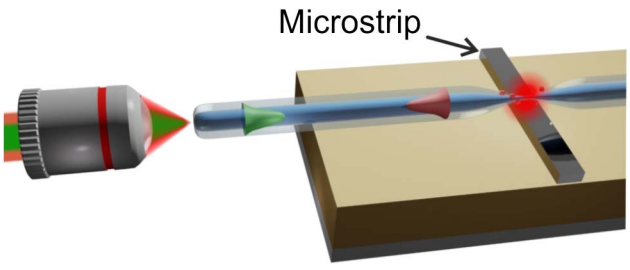

Fig. 2. Waveguide delivery of optical fields for the initialization and readout of the electron spin in NV centers using a nanodiamond-covered tapered fiber. The microwave field is delivered through a microstrip transmission line.

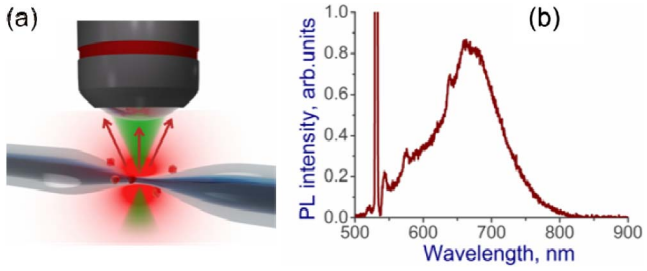

Fig. 3. Characterization of the PL response from NV centers in nanodiamond deposited on the fiber taper: (a) sketch of the experiment and (b) the spectrum of the PL response from NV centers in nanodiamond deposited on the fiber taper measured using a free-space 532-nm laser beam, as shown in panel (a).

the spectrum of background emission was subtracted from the spectra of the overall return signal delivered by the fiber probe to the detector.

The electron spin of the ground-state triplet of NV centers is manipulated in our scheme of fiber-based optical magnetometry using a microwave field, generated by a compact microwave source with a typical output power up to 0.5 W. The microwave field is delivered to the nanodiamond-covered fiber taper through a microstrip transmission line (Fig. 2), consisting of a 50-μm thick and 1-mm wide copper-foil strip on top of an Al_2O_3 substrate, which separates the strip from a copper ground-plane layer.

To separate the spin readout signal from the intense PL background, readily seen in Fig. 4(a), a rectangular modulation with a frequency $f_m \approx 1.13$ kHz is applied to the frequency of the microwave output using a digit-to-analog converter, controlled by homemade dedicated software. The frequency of the modulated microwave output changes periodically in a rectangular fashion from its minimum at 2.3 GHz to its maximum value scanned from 2.5 to 3.1 GHz. A lock-in amplifier is then used to retrieve a signal at $f_m \approx 1.13$ kHz from the overall PL return, thus discriminating the modulated spin readout against the constant PL background.

When tuned to the electron spin resonance (ESR) frequency Ω_s, the microwave field efficiently transfers population from the $m_s = 0$ to the $m_s = \pm 1$ state [Fig. 1(c)]. For NV centers in the $m_s = \pm 1$ state, the PL yield is lower than that typical of NV centers in the $m_s = 0$ state, because a substantial fraction of the $m_s = \pm 1$ excited-state population is transferred to the $m_s = 0$ ground level via a metastable singlet state (the ^1A state in [Fig. 1(c)]). This pathway does not contribute to the 630–800-nm PL band, allowing optical detection of ESR with the spin state readout from the intensity of the PL signal. An external magnetic field **B** removes the degeneracy of the $m_s = \pm 1$ state and induces a Zeeman frequency splitting $\Delta\Omega_Z$ between the $m_s = \pm 1$ sublevels [Fig. 1(c)].

In the case of a single NV center, when the spin-quantization axis has a well-defined orientation relative to an external magnetic field, these Zeeman-shifted sublevels are observed as well-resolved **B**-dependent features in the intensity of photoluminescence I_{PL} measured as a function of the microwave frequency Ω, making a single NV center an ideal quantum magnetometer. In an ensemble of randomly oriented NV centers, however, the

projection of the magnetic field on the spin quantization axis is different for individual NV centers [Fig. 1(a)]. As a result, the Zeeman-shifted components related to various orientations of NV centers are no longer resolved in the $I_{PL}(\Omega)$ spectrum, but merge together in an inhomogeneously broadened feature [Fig. 4(b)].

To understand how the magnetic field can be retrieved from such spectra, we resort to the spin Hamiltonian of an NV center [12–14], which, in the presence of an external magnetic field **B**, is written as $H_s = \mu_B g\mathbf{BS} + hD[S_z^2 - S(S+1)/3] + hE(S_x^2 - S_y^2)$, where μ_B is the Bohr magneton, h is the Planck constant, $g \approx 2$ is the electron g-ratio, D and E are the zero-magnetic-field splitting parameters, and $S_j (j = X, Y, Z)$ are the projections of the electron spin **S** on the principal Cartesian coordinate axes X, Y, Z, with the Z-axis chosen along the N-V axis. The first term in this Hamiltonian describes the Zeeman effect in an external magnetic field, which is observed against zero-field splitting due to the crystal field, governed by the second and third terms in H_s, dominated by the splitting $\Omega_s = D \approx 2.87$ GHz between the $m_s = 0$ spin state and the twofold-degenerate $m_s = \pm 1$ state.

The characteristic equation for the spin Hamiltonian H_s yields the following solution for the magnitude of the magnetic field [14]: $B^2 = h^2\mu_B^{-2} g^{-2}[(\Omega_1^2 + \Omega_2^2 - \Omega_1\Omega_2 - D^2)/3 - E^2]$, where Ω_1 and Ω_2 are the frequencies of the Zeeman-shifted ESR peaks in $I_{PL}(\Omega)$ spectra. Remarkably, while the frequencies Ω_1 and Ω_2 depend on the angle θ between the magnetic field **B** and the NV axis [Fig. 1(a)], the value of B dictated by each pair of Ω_1 and Ω_2 remains invariant. This property of the spin Hamiltonian allows the entire $I_{PL}(\Omega)$ spectrum measured for an ensemble of randomly oriented NV spins to be fitted (solid lines in the lower panel of Fig. 4(b)) using B as a single fitting parameter.

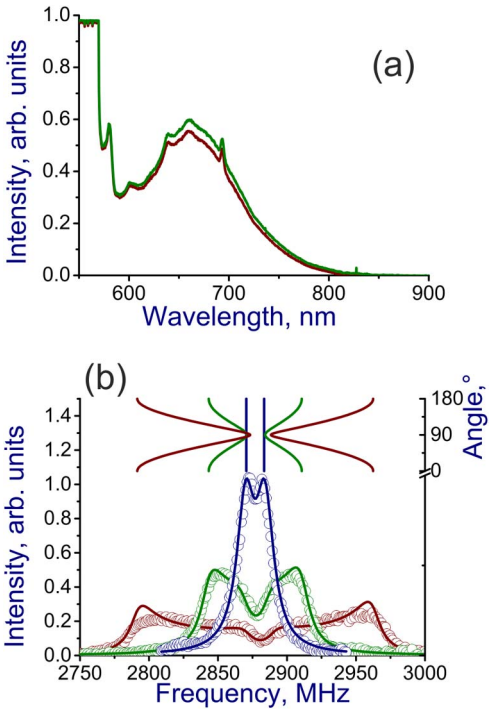

Fig. 4. (a) The spectrum of the PL response from NV centers in nanodiamond deposited on the fiber taper measured with a fiber delivery of both the 532-nm laser beam and the PL spin readout signal, as shown in Fig. 2, with an external magnetic field $B \approx 5$ mT (red line) and $B = 0$ (green line). (b) The spin readout return measured (circles) and calculated (solid lines) as a function of the frequency of the microwave field with both the 532-nm laser beam and the PL spin readout signal delivered through the tapered fiber for $B = 0$ (blue), 1.2 mT (green), and 3.0 mT (red). The upper panel shows the frequencies Ω_1 and Ω_2 calculated using the characteristic equation for H_s as functions of the angle θ between the magnetic field B and the axis of the NV center.

In Fig. 4(b), we present $I_{PL}(\Omega)$ spectra measured through the fiber-optic probe with a nanodiamond-covered fiber taper for different magnitudes of an external magnetic field. All these spectra are seen to broaden with increasing B and to feature a well-resolved dip at the center along with intense wings, followed by steep edges at large Ω. These properties of $I_{PL}(\Omega)$ spectra can be understood in terms of the characteristic equation of the spin Hamiltonian H_s, which allows two Ω solutions for each θ angle, defining two branches of the $\Omega(\theta)$ function (the upper plot in Fig. 4(b)), corresponding to the frequencies $\Omega_{1,2}$ of the Zeeman-split ESR pairs in the $I_{PL}(\Omega)$ spectrum. These two branches of the $\Omega(\theta)$ function are separated by a gap, which is mainly controlled by the D parameter (as $D \gg E$ in our case) and defines the zero-field splitting of the $I_{PL}(\Omega)$ spectrum. This gap translates into a dip, which is clearly resolved in the central part of all the experimental $I_{PL}(\Omega)$ spectra (the lower panel in [Fig. 4]).

In experiments, an external magnetic induces a noticeable shift of this gap, which is fully consistent with the properties of the $\Omega_{1,2}(\theta)$ solutions dictated by the characteristic equation of H_s (cf. the upper and lower panels in [Fig. 4(b)]). Steep outer edges of the $I_{PL}(\Omega)$ spectra at large Ω in Fig. 4(b), on the other hand, can be understood in terms of the density of $\Omega_{1,2}$ states in the θ phase space, controlled by the factor $d\Omega/d\theta$. As can be seen in the upper panel in Fig. 4(b), this derivative reaches its maximum at $\theta \approx 0, \pi$ for both branches of $\Omega(\theta)$, i.e., for NV spins parallel or antiparallel to the external magnetic field, providing the maximum density of $\Omega_{1,2}$ states per unit volume in the θ phase space.

Fast magnetic-field sensing is carried out in our experiments by extracting B from measurements performed at a single frequency Ω_0 corresponding to a maximum steepness of the $I_{PL}(\Omega)$ spectrum. For $B \approx 0.1$ mT, a fiber probe with a taper waist diameter of 1 μm and a taper length of 0.3 mm yields $(\partial I_{PL}/\partial\Omega)/\Omega_0 \approx 180$ μV/MHz. The standard deviation of the PL signal due to the overall noise is estimated as $\sigma \approx 75$ μV in this regime for measurements performed within a sampling time $\tau_s \approx 1$ s, which translates into an error of $\sigma/(\partial I_{PL}/\partial\Omega)/\Omega_0 \approx 0.4$ MHz in frequency definition and an uncertainty $\delta B \approx 16$ μT in the magnetic field. The sensitivity of magnetic-field measurements in this regime is thus estimated as $\eta \approx \delta B_e \tau_s^{1/2} \approx 16\ \mu\mathrm{T} \cdot \mathrm{Hz}^{-1/2}$. This sensitivity is noticeably higher than the sensitivities of magnetic-field measurements (57–58 $\mu\mathrm{T} \cdot \mathrm{Hz}^{-1/2}$) attainable with a single-NV-center tapered-fiber magnetometer [17]. Much higher sensitivities, at the level of a few $\mathrm{fT} \cdot \mathrm{Hz}^{-1/2}$, can be achieved with ensembles of oriented NV centers in diamond [12] and with magnetometers based on superconducting quantum interference devices (SQUIDs) [19].

However, the scheme of optical magnetometry demonstrated here offers significant advantages due to its ultracompact fiber-taper design and compatibility with ultrahigh-resolution fiber-tip scanning technologies.

The stability of the attachment of diamond nanoparticles to the fiber taper is verified by the PL intensity from NV centers collected from the fiber taper, which degraded by less than 10% within four months of measurements. This change in the PL intensity translated into a 10% lowering in the accuracy of magnetic field measurements. However, it did not give rise to any systematic errors in magnetic-field measurements.

Tapered-fiber probes with taper waist diameters ranging from 0.5 to 5 μm and taper lengths ranging from 0.05 to 3 mm yield different PL intensities in the optical readout. However, the magnetic fields retrieved from measurements performed with all these fiber probes vary only within the limits of experimental errors as specified above. As a consequence, variations in the ambient temperature change the PL intensity in the optical readout, but do not give rise to systematic errors in magnetic-field measurements beyond those resulting from the ≈75 kHz/K shift of the zero-field magnetic resonance [20].

To summarize, we have demonstrated that ensembles of randomly NV spins can enable a compact and practical scheme of optical magnetometry, which is ideally suited for fiber-format metrology and tip-assisted ultrahigh-resolution microscopy. In the scheme of optical magnetometry presented in this Letter, tapered optical fibers covered with NV-doped diamond nanoparticles are used as fiber probes, providing a waveguide delivery of optical fields for the initialization, polarization, and readout of the electron spin in NV centers.

This research was supported in part by the Russian Foundation for Basic Research (project nos. 13-02-92115, 13-04-40335, 14-02-90030, and 14-22-02100), the Welch Foundation (grant no. A-1801), and the National Science Foundation (grant no. 1202258). Research into the optics of tapered fibers has been supported by the Russian Science Foundation (project no. 14-12-00772).

References

1. T. Gaebel, M. Domhan, I. Popa, C. Wittmann, P. Neumann, F. Jelezko, J. R. Rabeau, N. Stavrias, A. D. Greentree, and S. Prawer, Nat. Phys. **2**, 408 (2006).
2. M. G. Dutt, L. Childress, L. Jiang, E. Togan, J. Maze, F. Jelezko, A. S. Zibrov, P. R. Hemmer, and M. D. Lukin, Science **316**, 1312 (2007).
3. I. Aharonovich, A. D. Greentree, and S. Prawer, Nat. Photonics **5**, 397 (2011).
4. A. P. Nizovtsev, S. Y. Kilin, F. Jelezko, T. Gaebal, I. Popa, A. Gruber, and J. Wrachtrup, Opt. Spectrosc. **99**, 233 (2005).
5. L. Childress, M. V. G. Dutt, J. M. Taylor, A. S. Zibrov, F. Jelezko, J. Wrachtrup, P. R. Hemmer, and M. D. Lukin, Science **314**, 281 (2006).
6. T. M. Babinec, B. J. Hausmann, M. Khan, Y. Zhang, J. R. Maze, P. R. Hemmer, and M. Lončar, Nat. Nanotechnol. **5**, 195 (2010).
7. A. Gruber, A. Dräbenstedt, C. Tietz, L. Fleury, J. Wrachtrup, and C. von Borczyskowski, Science **276**, 2012 (1997).
8. R. J. Epstein, F. M. Mendoza, Y. K. Kato, and D. D. Awschalom, Nat. Phys. **1**, 94 (2005).
9. G. Kucsko, P. C. Maurer, N. Y. Yao, M. Kubo, H. J. Noh, P. K. Lo, H. Park, and M. D. Lukin, Nature **500**, 54 (2013).
10. L. P. McGuinness, Y. Yan, A. Stacey, D. A. Simpson, L. T. Hall, D. Maclaurin, S. Prawer, P. Mulvaney, J. Wrachtrup, F. Caruso, R. E. Scholten, and L. C. Hollenberg, Nat. Nanotechnol. **6**, 358 (2011).
11. D. Le Sage, K. Arai, D. R. Glenn, S. J. DeVience, L. M. Pham, L. Rahn-Lee, M. D. Lukin, A. Yacoby, A. Komeili, and R. L. Walsworth, Nature **496**, 486 (2013).
12. J. M. Taylor, P. Cappellaro, L. Childress, L. Jiang, D. Budker, P. R. Hemmer, A. Yacoby, R. Walsworth, and M. D. Lukin, Nat. Phys. **4**, 810 (2008).
13. J. R. Maze, P. L. Stanwix, J. S. Hodges, S. Hong, J. M. Taylor, P. Cappellaro, L. Jiang, M. G. Dutt, E. Togan, A. S. Zibrov, A. Yacoby, R. L. Walsworth, and M. D. Lukin, Nature **455**, 644 (2008).
14. G. Balasubramanian, I. Y. Chan, R. Kolesov, M. Al-Hmoud, J. Tisler, C. Shin, C. Kim, A. Wojcik, P. R. Hemmer, A. Krueger, T. Hanke, A. Leitenstorfer, R. Bratschitsch, F. Jelezko, and J. Wrachtrup, Nature **455**, 648 (2008).
15. T. Schröder, A. W. Schell, G. Kewes, T. Aichele, and O. Benson, Nano Lett. **11**, 198 (2010).
16. I. V. Fedotov, N. A. Safronov, Y. A. Shandarov, A. A. Lanin, A. B. Fedotov, S. Y. Kilin, K. Sakoda, M. O. Scully, and A. M. Zheltikov, Appl. Phys. Lett. **101**, 031106 (2012).
17. X. Liu, J. Cui, F. Sun, X. Song, F. Feng, J. Wang, W. Zhu, L. Lou, and G. Wang, Appl. Phys. Lett. **103**, 143105 (2013).
18. I. V. Fedotov, L. V. Doronina-Amitonova, A. A. Voronin, A. O. Levchenko, S. A. Zibrov, D. A. Sidorov-Biryukov, A. B. Fedotov, V. L. Velichansky, and A. M. Zheltikov, Sci. Rep. **4**, 5362 (2014).
19. S. J. Bending, Adv. Phys. **48**, 449 (1999).
20. V. M. Acosta, E. Bauch, M. P. Ledbetter, A. Waxman, L.-S. Bouchard, and D. Budker, Phys. Rev. Lett. **104**, 070801 (2010).